CHALMERS
UNIVERSITY OF TECHNOLOGY

Finite-Element Based State-Space Modeling of AC Winding Losses in Synchronous Machines

Downloaded from: https://research.chalmers.se, 2026-11-14 20:43 UTC

Citation for the original published paper (version of record):
Abbas, A., Vesa, J., Marjamäki, A. et al (2026). Finite-Element Based State-Space Modeling of AC Winding Losses in Synchronous Machines. IEEE Transactions on Magnetics, 62(7). http://dx.doi.org/10.1109/TMAG.2025.3608315

N.B. When citing this work, cite the original published paper.

© 2026 IEEE. Personal use of this material is permitted. Permission from IEEE must be obtained for all other uses, in any current or future media, including reprinting/republishing this material for advertising or promotional purposes, or reuse of any copyrighted component of this work in other works.

(article starts on next page)

Finite-Element-Based State-Space Modeling of AC Winding Losses in Synchronous Machines

Amr A. Abbas[1,2], Joonas Vesa[1], Antero Marjamäki[1], Hadhiq Khan[1], Yujing Liu[3], and Paavo Rasilo[1]

[1]Electrical Engineering Unit, Tampere University, 33720 Tampere, Finland
[2]Department of Electrical Engineering, Cairo University, Giza 12613, Egypt
[3]Department of Electrical Engineering, Chalmers University of Technology, 41296 Gothenburg, Sweden

This article proposes a finite element (FE) based state-space model for evaluating AC winding losses in synchronous machines to be implemented in Simulink. The model is constructed by storing multiple static FE solutions into lookup-tables to express the magnetic vector potential on the boundaries of the stator slot region as a function of stator currents and rotor position. The geometry-dependent FE matrices derived from the slot mesh are computed only once, while the dynamic simulation evaluates AC winding losses at each time step based on the instantaneous operating conditions. The model allows using arbitrary voltage excitations such as sinusoidal and pulsewidth modulated supplies seamlessly without the need of pre-computing the harmonic content of the current waveform. Proper orthogonal decomposition is used to reduce the model complexity and speed up the simulation. The Simulink implementation of the proposed AC winding loss model shows good agreement with the time-stepping FE simulation results, while achieving a 60-fold speedup in computation.

***Index Terms*— AC losses, model order reduction, state-space model, synchronous machine, windings.**

I. Introduction

AC WINDING losses are a significant source of power loss in electrical machines, particularly at high operating speeds. Accurate modeling of these losses is essential for evaluating machine efficiency over an extended operating range, such as during a full driving cycle simulation.

The calculation methods for AC winding losses can be broadly classified into four categories [1]: finite element-based models [2], [3], [4], [5], analytical models [6], [7], [8], [9], [10], hybrid models [11], [12], [13], and experiment-based models [14]. FE-based models provide highly accurate results, but are computationally intensive and impractical for long dynamic simulations. Analytical models offer fast calculations, but their accuracy is often compromised due to inherent assumptions and approximations. Hybrid models try to combine the strengths of both approaches by solving FE simulations at selected operating points and use the analytical techniques to generalize the results across a wider range of operating conditions.

Different challenges can be identified in the existing literature on AC winding loss calculation, particularly in accounting for losses under pulsewidth modulated (PWM) supply and in achieving a balance between accuracy and computational efficiency. The models in [2], [7], [8], [9], [10], [11], and [13] consider only the AC loss calculation for the fundamental frequency with sinusoidal supply. The impact of PWM excitation on AC losses has received less attention in the literature [6], [12], [15]. In these studies, the general approach involves extracting the current waveform, decomposing it into its harmonic components, and then computing the AC loss for each harmonic separately. The total loss is subsequently estimated by summing the individual contributions using the superposition principle. However, this approach limits the applicability of such models in dynamic simulations, where the current waveform continuously changes with the operating conditions.

An FE-based state-space model for synchronous machines including core loss is introduced in [16]. This model is constructed by solving multiple static FE simulations to represent the winding flux linkages and the flux-density distribution in the FE integration points as functions of stator currents and rotor angle and storing them into lookup-tables (LUTs). The model demonstrated good accuracy and fast execution time when implemented in Simulink.

In this article, the SS model is extended with a winding loss model that accounts for skin and proximity effects in the solid stator conductors under any arbitrary voltage excitations. However, since such winding phenomena involve internal states due to eddy currents, the SS model based on static FE solutions is not sufficient to model these effects. Therefore, additional states are introduced. The winding loss model is a 2-D FE formulation of a single slot coupled with the circuit equations of the stator winding. The resulting differential-algebraic equation (DAE) system can be implemented as a computationally efficient subsystem in Simulink. The winding loss model is driven by the instantaneous conductor currents and the vector potential values on the boundary of the slot. These boundary values are pre-computed from static FE solutions and stored in a separate LUT as functions of stator currents and rotor position. In addition, the proper orthogonal decomposition technique is used to reduce the model complexity and accelerate the simulation.

The structure of the article is as follows. Section II-A provides a brief overview of the machine SS model. The

Received 30 June 2025; revised 1 September 2025; accepted 7 September 2025. Date of publication 10 September 2025; date of current version 13 July 2026. Corresponding author: A. A. Abbas (e-mail: amr.abbas@tuni.fi).

Color versions of one or more figures in this article are available at https://doi.org/10.1109/TMAG.2025.3608315.

Digital Object Identifier 10.1109/TMAG.2025.3608315

© 2025 The Authors. This work is licensed under a Creative Commons Attribution 4.0 License.
For more information, see https://creativecommons.org/licenses/by/4.0/

formulation and implementation of the AC loss model are discussed in Section II-B, followed by the application of the POD technique in Section II-C. Section III-A presents the application of the proposed AC loss model to the test machine, while the verification against the time-stepping FE simulation is presented in Section III-B. Finally, Section IV presents the conclusions of the article.

II. Methods

A. Machine SS Model

A brief overview of the motor SS model is provided here. The complete derivation can be found in [16]. In isolated star-connected machines, the sum of the phase currents is zero and each line-to-line voltage acts over two phase windings. For a three-phase machine, this can be formulated in a matrix form as

$$\boldsymbol{i}_{\mathrm{abc}} = \boldsymbol{K}^{\mathrm{T}}\boldsymbol{i}_{\mathrm{ab}}, \quad \boldsymbol{K}\boldsymbol{u}_{\mathrm{abc}} = \boldsymbol{Q}\boldsymbol{U}_{123} \tag{1}$$

where column vector $\boldsymbol{i}_{\mathrm{abc}}$ contains the phase currents, $\boldsymbol{u}_{\mathrm{abc}}$ and $\boldsymbol{U}_{123}$ contain the stator phase and line-to-line voltages, respectively, and $\boldsymbol{Q}$ and $\boldsymbol{K}$ are connection matrices given by

$$\boldsymbol{Q} = \begin{bmatrix} 0 & 0 & -1 \\ -1 & 0 & -1 \end{bmatrix}, \quad \boldsymbol{K} = \begin{bmatrix} 1 & 0 & -1 \\ 0 & 1 & -1 \end{bmatrix}. \tag{2}$$

The machine SS model is then expressed as

$$\frac{d\boldsymbol{i}_{\mathrm{ab}}}{dt} = \left(\frac{\partial\left(\boldsymbol{K}\boldsymbol{\psi}_{\mathrm{abc}}\right)}{\partial \boldsymbol{i}_{\mathrm{ab}}}\right)^{-1}\left[\boldsymbol{Q}\boldsymbol{U}_{123} - R_{\mathrm{s}}\boldsymbol{K}\boldsymbol{K}^{\mathrm{T}}\boldsymbol{i}_{\mathrm{ab}} - \boldsymbol{K}\frac{\partial\left(\boldsymbol{K}\boldsymbol{\psi}_{\mathrm{abc}}\right)}{\partial\alpha}\omega\right] \tag{3}$$

where $\boldsymbol{\psi}_{\mathrm{abc}}$ contains the stator flux linkages, R_{s} is the stator phase resistance, α is the electrical rotor position angle and $\omega = d\alpha/dt$ is the rotor electrical speed. The flux linkages $\boldsymbol{\psi}_{\mathrm{abc}}$ are obtained from multiple static FE simulations as functions of the stator currents and rotor position and stored in LUTs.

B. AC Winding Loss Model

1) Model Description: The proposed model for AC winding loss calculation is developed in two pre-computing stages. In the first stage, the FE matrices corresponding to the slot cross section are assembled based on the slot geometry and material properties. In the second stage, an LUT for Dirichlet boundary conditions is constructed from the static FE solutions.

The FE system for a slot filled with magnetically linear conductors and insulating material can be written as

$$\begin{bmatrix} \boldsymbol{T}_{\mathrm{cc}} & 0 & 0 \\ 0 & 0 & 0 \\ -\boldsymbol{F}^{\mathrm{T}} & 0 & 0 \end{bmatrix}\frac{d}{dt}\begin{bmatrix} \boldsymbol{a}_{\mathrm{c}} \\ \boldsymbol{a}_{\mathrm{n}} \\ \boldsymbol{e} \end{bmatrix} = \begin{bmatrix} -\boldsymbol{S}_{\mathrm{cc}} & -\boldsymbol{S}_{\mathrm{cn}} & \boldsymbol{F} \\ -\boldsymbol{S}_{\mathrm{nc}} & -\boldsymbol{S}_{\mathrm{nn}} & 0 \\ 0 & 0 & -l_{\mathrm{z}}/R \end{bmatrix}\begin{bmatrix} \boldsymbol{a}_{\mathrm{c}} \\ \boldsymbol{a}_{\mathrm{n}} \\ \boldsymbol{e} \end{bmatrix} + \begin{bmatrix} -\boldsymbol{S}_{\mathrm{cd}} & 0 \\ -\boldsymbol{S}_{\mathrm{nd}} & 0 \\ 0 & \boldsymbol{I} \end{bmatrix}\begin{bmatrix} \boldsymbol{a}_{\mathrm{d}} \\ \boldsymbol{i} \end{bmatrix} \tag{4}$$

where $\boldsymbol{a}_{\mathrm{c}}$ and $\boldsymbol{a}_{\mathrm{n}}$ contain the nodal values of the vector potential in the conductors and the non-conducting regions, respectively, $\boldsymbol{e}$ contains the out-of-plane components of the electric fields in the conductors, $\boldsymbol{S}_{\mathrm{cc}}$, $\boldsymbol{S}_{\mathrm{nn}}$, $\boldsymbol{S}_{\mathrm{cn}}$, and $\boldsymbol{S}_{\mathrm{nc}}$ contain the parts of the stiffness matrix corresponding to conducting and non-conducting regions and their interfaces, $\boldsymbol{T}_{\mathrm{cc}}$ contains the parts of the damping matrix corresponding to conducting regions, $\boldsymbol{F}$ is a matrix for imposing the field sources and calculating the induced voltages in the conductors, $\boldsymbol{S}_{\mathrm{cd}}$ and $\boldsymbol{S}_{\mathrm{nd}}$ are the stiffness matrix parts corresponding to the Dirichlet boundary values, $\boldsymbol{I}$ is the identity matrix, $\boldsymbol{a}_{\mathrm{d}}$ and $\boldsymbol{i}$ contain the Dirichlet conditions and the conductor currents that are used as inputs, R contains the dc resistances of the conductor regions, and l_{z} is the out-of-plane length. For loss calculations, $d\boldsymbol{a}_{\mathrm{c}}/dt$ and $\boldsymbol{e}$ can be obtained as

$$\begin{bmatrix} \frac{d\boldsymbol{a}_{\mathrm{c}}}{dt} \\ \boldsymbol{e} \end{bmatrix} = \begin{bmatrix} -\boldsymbol{T}_{\mathrm{cc}}^{-1}\boldsymbol{S}_{\mathrm{cc}} & -\boldsymbol{T}_{\mathrm{cc}}^{-1}\boldsymbol{S}_{\mathrm{cn}} & \boldsymbol{T}_{\mathrm{cc}}^{-1}\boldsymbol{F} \\ 0 & 0 & \boldsymbol{I} \end{bmatrix}\begin{bmatrix} \boldsymbol{a}_{\mathrm{c}} \\ \boldsymbol{a}_{\mathrm{n}} \\ \boldsymbol{e} \end{bmatrix} + \begin{bmatrix} -\boldsymbol{T}_{\mathrm{cc}}^{-1}\boldsymbol{S}_{\mathrm{cd}} & 0 \\ 0 & 0 \end{bmatrix}\begin{bmatrix} \boldsymbol{a} \\ \boldsymbol{i} \end{bmatrix}. \tag{5}$$

Once the system is solved, the eddy-current loss per unit length in the conductors is computed as

$$p = \begin{bmatrix} \frac{d\boldsymbol{a}_{\mathrm{c}}}{dt} \\ \boldsymbol{e} \end{bmatrix}^{\mathrm{T}}\begin{bmatrix} \boldsymbol{T}_{\mathrm{cc}} & -\boldsymbol{F} \\ -\boldsymbol{F}^{\mathrm{T}} & l_{\mathrm{z}}/R \end{bmatrix}\begin{bmatrix} \frac{d\boldsymbol{a}_{\mathrm{c}}}{dt} \\ \boldsymbol{e} \end{bmatrix}. \tag{6}$$

Systems (6) to (4) can be expressed in the descriptor SS form as

$$\boldsymbol{E}\frac{d\boldsymbol{x}}{dt} = \boldsymbol{A}\boldsymbol{x} + \boldsymbol{B}\boldsymbol{u} \tag{7a}$$

$$\boldsymbol{y} = \boldsymbol{C}\boldsymbol{x} + \boldsymbol{D}\boldsymbol{u} \tag{7b}$$

$$p = \boldsymbol{y}^{\mathrm{T}}\boldsymbol{G}\boldsymbol{y} \tag{7c}$$

which can be straightforwardly implemented in Simulink. These matrices are computed once beforehand and subsequently used during the dynamic simulation. It is worth noting that these matrices depend only on the slot geometry and material parameters and are independent of the operating conditions of the simulation.

Besides the FE matrices of the slot, Dirichlet conditions $\boldsymbol{a}_{\mathrm{d}}$ of the slot region are needed as an input to the model (7). These values are pre-computed from the static FE solutions and stored in a separate LUT as functions of stator current and rotor angle. During the dynamic simulation, these values are interpolated and fed to the model alongside the slot current.

2) Implementation: Two different approaches can be used to implement the DAE system (7) in Simulink. The first is to use the Descriptor SS block and provide matrices $\boldsymbol{E}$, $\boldsymbol{A}$, $\boldsymbol{B}$, $\boldsymbol{C}$, and $\boldsymbol{D}$ to it directly. However, it turns out that the behavior of this block depends on the choice of the time-stepping solver and can sometimes lead to instabilities in the simulation. Therefore, system (7) is implemented using the basic Simulink blocks by discretizing it manually with the backward Euler method. Equation (7a) becomes

$$\boldsymbol{E}\frac{\boldsymbol{x}^{k} - \boldsymbol{x}^{k-1}}{\Delta t} = \boldsymbol{A}\boldsymbol{x}^{k} + \boldsymbol{B}\boldsymbol{u}^{k} \tag{8}$$

where Δt is the time-step length and the superscripts denote discrete time indices. The value of the state vector $\boldsymbol{x}$ at time step k is obtained as

$$\boldsymbol{x}^{k} = \left(\frac{\boldsymbol{E}}{\Delta t} - \boldsymbol{A}\right)^{-1}\left(\frac{\boldsymbol{E}}{\Delta t}\boldsymbol{x}^{k-1} + \boldsymbol{B}\boldsymbol{u}^{k}\right). \tag{9}$$

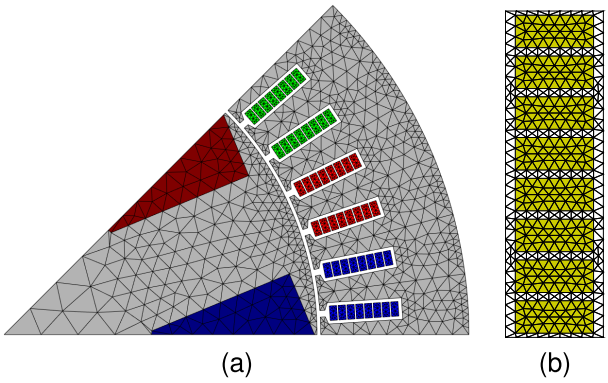

Fig. 1. FE mesh of the machine under study. (a) FE mesh of 1/8 segment of the machine with 1476 elements and 871 nodes. (b) FE mesh of the slot with 8 solid conductors.

This implementation is valid for both fixed-step and variable-step solvers. Once $\boldsymbol{x}^k$ is obtained, the output equation (7b) and the power loss expression (7c) are evaluated at each time step to compute the instantaneous eddy-current loss per unit length.

C. Model Order Reduction

POD is employed to reduce the computation cost of the proposed AC winding loss model [17]. A snapshot matrix $\boldsymbol{X}$ is first constructed by solving the full order model (FOM) at a range of different operating points and storing the state vector $\boldsymbol{x}$. POD is then applied to each component in $\boldsymbol{x}$ independently to choose the dominant modes of each component. Singular value decomposition (SVD) is used to obtain these modes by factorizing $\boldsymbol{X}$ to three matrices

$$\boldsymbol{X} = \boldsymbol{U}\Sigma\boldsymbol{V}^{\mathrm{T}} \tag{10}$$

where $\boldsymbol{U}$ and $\boldsymbol{V}$ are orthonormal matrices containing the left and right singular vectors, respectively, and Σ is a diagonal matrix containing the singular values sorted in a descending order. The columns of $\boldsymbol{U}$ represent the POD modes and the elements of Σ represent their significance.

Since most of the system dynamics are captured by the first few modes, the SVD is truncated to retain only these significant modes. These dominant modes serve as a reduced basis to project the FOM onto a lower dimensional subspace. The reduced order model (ROM) is then constructed by applying this reduced basis to the FOM matrices.

III. Application and Results

A. Application

The proposed model is verified against a 2-D time-stepping FE simulation in the case of a 200 kW electrically excited synchronous motor equipped with eight solid conductors per slot. The model is supplied with both sinusoidal and PWM voltage supplies and constant field current. The static and time-stepping simulations are carried out using in-house MATLAB-based FE solvers. Fig. 1(a) shows the FE mesh of the modeled sector of the machine, while Fig. 1(b) shows the mesh of a single slot with eight solid conductors. The machine parameters are listed in Table I.

TABLE I
Parameters of the Machine Under Study

Parameter	Value
Rated shaft power	200 kW
Rated voltage	537 V
Rated frequency	200 Hz
Rated current	255 A
Phase resistance	20 mΩ
Number of poles	8
Number of slots	48
Stator axial length	200 mm
Stator outer diameter	258 mm

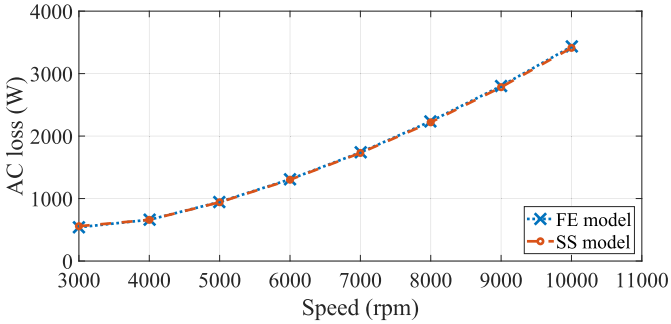

Fig. 2. Comparison between the FE model and SS model under sinusoidal supply.

A separate model is constructed for each individual slot within the symmetry sector in Fig. 1(a). The inputs to the model are the Dirichlet conditions and the currents. The Dirichlet values are obtained from the pre-computed LUT, while the stator current is solved as a state in the SS model. These inputs are fed to each slot model independently. The total loss is then obtained by summing up the loss for those six slots and multiplying by the number of symmetry sectors and the axial length of the machine. Subsequently, the AC loss P_{ac} is obtained as the difference between the total loss P_{tot} and the dc copper loss. Throughout the simulation, the operating point is selected to maintain constant output mechanical power and stator current magnitude at different speeds, ensuring a fair comparison of the AC winding losses.

B. Results

In this section, a comparison between the proposed model and the time-stepping FE simulation under both sinusoidal and PWM excitations is presented. Fig. 2 compares the AC loss obtained from the FE model and the SS model at different speeds under sinusoidal supply. It can be seen that as the speed increases, the AC loss increases as expected. Moreover, the proposed AC loss model shows close agreement with the FE results across the entire speed range. Fig. 3 shows a comparison between the two models under PWM supply at a fixed switching frequency of 10 kHz. The results again indicate a good agreement between the two models. Together, these two figures demonstrate that the proposed AC loss model provides an accurate representation of the FE results.

A key advantage of the proposed model is its capability to calculate the AC loss due to PWM supply directly, without the need for prior harmonic analysis of the current waveform

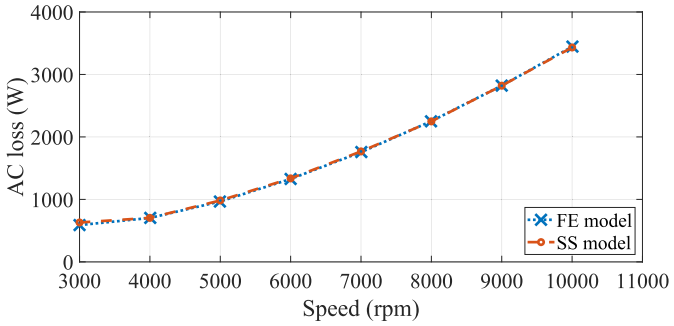

Fig. 3. Comparison between the FE model and SS model under PWM supply.

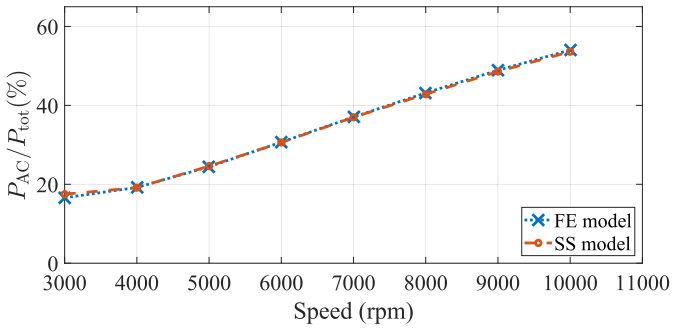

Fig. 4. AC loss as a percentage of the total copper loss under PWM supply.

TABLE II
AC LOSS AT DIFFERENT m_f

m_f	5	10	25	50	75	105	Sinusoidal
P_{ac}(W)	710	659	614	589	573	563	540

or superposition of individual harmonic losses [6], [12], [15]. In that case, the PWM supply is treated seamlessly, in the same manner as a sinusoidal supply. The effect of PWM supply on the AC loss value is relatively minor compared to the impact of speed increasing, similar to the result in [15].

Fig. 4 shows the AC loss as a percentage of the total copper loss at different speeds. Around the rated speed, the AC loss accounts for approximately 20% of the total copper loss. However, as the speed increases, the AC loss dominates the dc loss reaching approximately 60% of the total copper loss at the maximum speed. This figure highlights the importance of accurately modeling the AC winding losses, particularly in high-speed operation.

The switching frequency can affect the AC loss. To investigate this effect, the frequency modulation ratio (m_f), that is defined as the ratio between the switching and fundamental frequencies, is varied from low to high values at a fundamental frequency of 200 Hz. The corresponding AC loss values are reported in Table II, while the corresponding current waveforms at these m_f values are shown in Fig. 5. As shown in the figure, the current waveform is distorted at low values of m_f, indicating a high harmonic content and consequently higher AC loss values. As m_f increases, the harmonic content decreases, and the AC loss also correspondingly decreases.

The computational time of the proposed approach can be divided into two stages: a pre-computation stage and

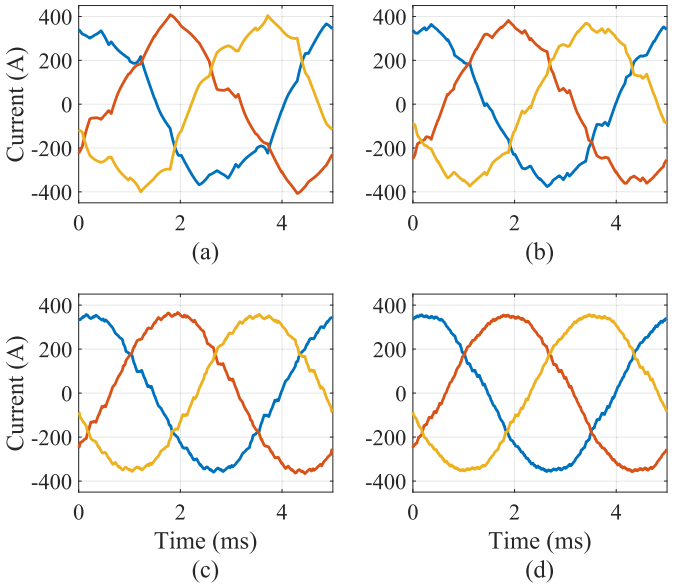

Fig. 5. Current waveforms at different m_f values. (a) $m_f = 5$ (b) $m_f = 10$. (c) $m_f = 25$. (d) $m_f = 50$.

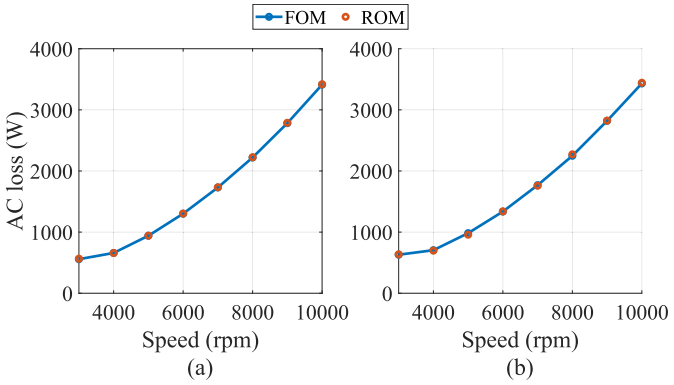

Fig. 6. AC winding loss obtained from FOM and ROM. (a) Sinusoidal supply. (b) PWM supply.

a simulation stage. In the pre-computation stage, the machine LUTs are constructed, the vector potential values at the slot boundary are obtained, and the FE matrices of the slot region are assembled. For the grid data equal to the one mentioned in [16], this process requires approximately 85 min, but it is carried out only once.

In the simulation stage, the FE model requires about 65 ms per time step, whereas the Simulink implementation of the FOM requires approximately 40 ms per time step. Although this reduction is not substantial, the Simulink implementation offers flexibility in integrating different inverter topologies, modulation strategies, and control schemes. Furthermore, the computational burden can be greatly reduced through model order reduction.

To reduce the computational burden of the proposed model implementation, POD is employed. The snapshot matrix is first constructed by running the FOM at different speeds and storing the state vector $\boldsymbol{x}$ at each time step. POD is then applied to each component of $\boldsymbol{x}$ independently to pick the dominant modes. Fig. 6 compares the AC loss obtained

TABLE III
SIMULATION TIME PER STEP FOR EACH MODEL

Model	ROM	FOM	FE
Simulation time per step (ms)	1.1	40	65

from the ROM to the one obtained from the FOM under both sinusoidal and PWM excitations. The results show good agreement in both cases, indicating that the two models are consistent. Furthermore, the comparison highlights that the accuracy of the ROM is not affected by the supply waveform.

In terms of performance, the ROM implementation only requires 1.1 ms per time step, making it 36 times faster than the FOM implementation and nearly 60 times faster than the FE model. Table III summarizes the computation times for all three models.

IV. CONCLUSION

This article presented an FE-based SS model for evaluating AC winding losses in stator solid conductors of synchronous machines under both sinusoidal and PWM excitations. The model couples a 2-D FE formulation of a single slot with the stator circuit equations and is constructed in two pre-computed stages: first, by obtaining the geometry-dependent matrices from the slot mesh; and second, by storing the Dirichlet boundary values of the slot region in an LUT. A key feature of the proposed approach is its ability to calculate the AC loss due to PWM excitations directly without requiring prior harmonic analysis of the current waveform. Model order reduction using POD significantly reduces the computational burden. The results show good agreement with the full-time-stepping FE simulations while achieving a 60-fold reduction in the simulation time. This model is well-suited for long driving-cycle simulation of traction applications and allows for assessing the impact of modulation and control strategies on the AC winding losses.

ACKNOWLEDGMENT

This work is funded by the European Union's Horizon 2021 under grant number 101056857. Views and opinions expressed are however those of the author(s) only and do not necessarily reflect those of the European Union or the European Climate, Infrastructure and Environment Executive Agency (CINEA). Neither the European Union nor the granting authority can be held responsible for them. This project has also received funding from the European Research Council (ERC) under the European Union's Horizon 2020 research and innovation programme (grant agreement No 848590). The Academy of Finland is also acknowledged for financial support (grant No 346440).

REFERENCES

[1] T. E. Hajji et al., "AC losses in windings: Review and comparison of models with application in electric machines," *IEEE Access*, vol. 12, pp. 1552–1569, 2024.

[2] P. Mellor, R. Wrobel, and N. McNeill, "Investigation of proximity losses in a high speed brushless permanent magnet motor," in *Proc. Conf. Rec. IEEE Ind. Appl. Conf. 41st IAS Annu. Meeting*, vol. 3, Tampa, FL, USA, Oct. 2006, pp. 1514–1518.

[3] S. Iwasaki, R. P. Deodhar, Y. Liu, A. Pride, Z. Q. Zhu, and J. J. Bremner, "Influence of PWM on the proximity loss in permanent-magnet brushless AC machines," *IEEE Trans. Ind. Appl.*, vol. 45, no. 4, pp. 1359–1367, Jul. 2009.

[4] A. Lehikoinen, J. Ikäheimo, A. Arkkio, and A. Belahcen, "Domain decomposition approach for efficient time-domain finite-element computation of winding losses in electrical machines," *IEEE Trans. Magn.*, vol. 53, no. 5, pp. 1–9, May 2017.

[5] R. Schneckenleitner and P. Rasilo, "Model order reduction for multi-strand electrical machine windings," *IEEE Trans. Magn.*, vol. 60, no. 9, pp. 1–7, Sep. 2024.

[6] L. D. Leonardo, M. Popescu, and M. Villani, "Eddy-current losses evaluation in hairpin wound motor fed by PWM inverter," in *Proc. IECON 46th Annu. Conf. IEEE Ind. Electron. Soc.*, Singapore, Oct. 2020, pp. 943–948.

[7] Y. Du, Y. Huang, B. Guo, F. Peng, Y. Yao, and J. Dong, "Hybrid analytical model for AC copper loss computation of hairpin winding," *IEEE Trans. Magn.*, vol. 60, no. 3, pp. 1–4, Mar. 2024.

[8] N. Taran, D. M. Ionel, V. Rallabandi, G. Heins, and D. Patterson, "An overview of methods and a new three-dimensional FEA and analytical hybrid technique for calculating AC winding losses in PM machines," *IEEE Trans. Ind. Appl.*, vol. 57, no. 1, pp. 352–362, Jan. 2021.

[9] L. J. Wu and Z. Q. Zhu, "Simplified analytical model and investigation of open-circuit AC winding loss of permanent-magnet machines," *IEEE Trans. Ind. Electron.*, vol. 61, no. 9, pp. 4990–4999, Sep. 2014.

[10] H. Igarashi, "Semi-analytical approach for finite-element analysis of multi-turn coil considering skin and proximity effects," *IEEE Trans. Magn.*, vol. 53, no. 1, pp. 1–7, Jan. 2017.

[11] S.-H. Park, J.-W. Chin, K.-S. Cha, J.-Y. Ryu, and M.-S. Lim, "Investigation of AC copper loss considering effect of field and armature excitation on IPMSM with hairpin winding," *IEEE Trans. Ind. Electron.*, vol. 70, no. 12, pp. 12102–12112, Dec. 2023.

[12] X. Fan, D. Li, W. Kong, L. Cao, R. Qu, and Z. Yin, "Fast calculation of strand eddy current loss in inverter-fed electrical machines," *IEEE Trans. Ind. Electron.*, vol. 70, no. 5, pp. 4640–4650, May 2023.

[13] A. Fatemi, D. M. Ionel, N. A. O. Demerdash, D. A. Staton, R. Wrobel, and Y. C. Chong, "Computationally efficient strand eddy current loss calculation in electric machines," *IEEE Trans. Ind. Appl.*, vol. 55, no. 4, pp. 3479–3489, Jul. 2019.

[14] R. Wrobel, D. E. Salt, A. Griffo, N. Simpson, and P. H. Mellor, "Derivation and scaling of AC copper loss in thermal modeling of electrical machines," *IEEE Trans. Ind. Electron.*, vol. 61, no. 8, pp. 4412–4420, Aug. 2014.

[15] G. Volpe, M. Popescu, L. di Leonardo, and S. Xue, "Efficient calculation of PWM AC losses in hairpin windings for synchronous BPM machines," in *Proc. IEEE Int. Electric Mach. Drives Conf. (IEMDC)*, Hartford, CT, USA, May 2021, pp. 1–5.

[16] A. A. Abbas, J. Vesa, H. Khan, H. Chen, Y. Liu, and P. Rasilo, "Fast and accurate non-linear model for synchronous machines including core losses," *IEEE Trans. Energy Convers.*, vol. 39, no. 4, pp. 2559–2567, Dec. 2024.

[17] M. Farzamfar, A. Belahcen, P. Rasilo, S. Clenet, and A. Pierquin, "Model order reduction of electrical machines with multiple inputs," *IEEE Trans. Ind. Appl.*, vol. 53, no. 4, pp. 3355–3360, Jul. 2017.